Hindawi
International Journal of Rotating Machinery
Volume 2021, Article ID 9986733, 14 pages
https://doi.org/10.1155/2021/9986733

Research Article

Experimental Research on the Similarity of Rime Icing on a Cylinder Rotating around Its Horizontal Axis

Lei Shi,[1,2] **Yan Li**,[1] **Wenfeng Guo**,[1] **and Ce Sun**[1]

[1]*College of Engineering, Northeast Agricultural University, Harbin 150030, China*
[2]*College of Mechanical and Electrical Engineering, Hebei Normal University of Science and Technology, Qinhuangdao 066600, China*

Correspondence should be addressed to Yan Li; liyanneau@163.com

Received 19 March 2021; Revised 23 September 2021; Accepted 12 October 2021; Published 8 November 2021

Academic Editor: Kenneth Van Treuren

Ice accumulation on the blade of a wind turbine surface seriously threatens the operational safety of the turbine; therefore, the research on this problem is very important. In this paper, a new similarity criterion of icing shape for a rotational model was proposed based on the similarity criterion for translational motion models in the aviation field, and experimental studies on the similarity of the rotational model icing were carried out. To validate the similarity criterion, icing wind tunnel tests were carried out with aluminum cylinders with diameters of 40 mm and 20 mm. Key parameters for the experiment, such as wind speed, temperature, liquid water content, medium volume diameter, and test time, were selected based on the criterion. All the icing tests were carried out in a new self-designed icing wind tunnel test system based on natural low-temperature conditions. The icing shapes observed in the tests were confirmed after many repetitions. To quantitatively analyze the similarity between different sizes of ice shapes, a dimensionless method for evaluating the similarity of ice shapes of different sizes was defined based on the typical characteristics of ice shapes. The research results show that the similarity score between two sizes of ice shapes under different test conditions is 81%~90%. The accuracy and applicability of the icing shape similarity criterion were thus validated. The research results in this paper lay a theoretical and experimental foundation for exploring the icing shape similarity of a rotating model.

1. Introduction

A wind turbine, when operating in low-temperature and humid environments, collides with supercooled water droplets in the air. Then, ice is generated on the surface of the turbine blades [1–5]. Ice on the surface of wind turbine blades changes the characteristics of the blades, such as the aerodynamic performance, mass distribution, and surface morphology. This reduces the power generation efficiency of the wind turbine. In some cases, ice on the rotating blade even threatens its safe operation, as observed with a helicopter propeller and engine intake of an airplane [3–10]. Presently, the methods of researching icing characteristics include icing wind tunnel tests and numerical simulation [11–13]. The icing wind tunnel test is an effective method for researching icing rotating machines. This test can provide fundamental data to validate theoretical research and numerical simulations. However, an icing wind tunnel in the lab hardly simulates the large size of a rotating machine. Therefore, in the aeronautic field, a similarity criterion is used to scale the large size of a model into a small model and test it in either an icing wind tunnel or numerically [14]. However, most of the research methods involve translational motion models, such as aircraft wings, and there has been a wide range of understanding and well-developed research methods for plane wing icing. Well-known icing similarity criteria for translational motion models include the AEDC criterion proposed by the American Arnold Engineering Development Center (AEDC) and the ONERA criterion proposed by the French Space Agency [15, 16]. Each criterion has its own characteristics and application conditions according to the research object. However, for surface icing under rotating conditions, there are obvious deficiencies in research methods, and a convincing similarity criterion for rotating icing has

not yet been developed to guide icing tests and calculations. Few studies on the icing similarity theory of rotating models, such as wind turbine blades, have been carried out. Therefore, expanding the application range of the icing similarity criterion to rotating models is needed. Han et al. used the AEDC criterion proposed by Ruff to conduct icing similarity tests on the rotor of a wind turbine (model NREL Phase VI) [12]. Experiments were carried out on rime ice and glaze ice. The results showed that to a certain extent, icing shapes of different scales have similarities under different working conditions. According to studies on the similarity criterion of icing shape for translational motion models and rotating models, the characteristics and mechanisms of icing by glaze ice and rime ice were of obvious difference.

Icing similarity problems include complex aerodynamic processes, such as droplet impingement, flow phase transition, heat and mass transfer, and dynamic growth of ice accretion. Presently, there are still many deficiencies in understanding these problems, which need to be explored further. In addition, academic research on the icing similarity theory of the rotating state is still in its initial stages. As the icing similarity theory of aircraft wings is relatively well developed, based on the static icing similarity theory of wings, this paper discusses the droplet trajectory, impact characteristics, surface impact water quantity, and heat mass transfer characteristics of wind turbine blade icing under rotating conditions and develops a set of universal dynamic and static icing similarity criterion. For cases of rotational model icing under dynamic conditions, only additional rotation similarity parameters can be considered.

In this paper, research on the similarity criterion of icing shape on a rotating cylinder surface under rime ice conditions was carried out. A set of parameters was selected based on the Weber number of the water film thickness, which was suitable for the similarity criterion under rime ice conditions, and the tensile stress generated by the centrifugal force was supplemented as a similarity parameter describing the rotating state. Similarity experiments on the icing shapes of rotating aluminum cylinders with different sizes in an icing wind tunnel were carried out. A set of parameters used to evaluate the ice shape similarity is defined. Thus, a set of ice similarity methods for rotating conditions was formed. Additionally, to determine the icing similarity under two different scales and to quantitatively analyze this similarity, this paper also studies a set of icing similarity evaluation methods. Different scales of rime icing shapes on cylinder surfaces were quantitatively analyzed. The significance of this study lies in the establishment of a novel icing shape similarity theory and the formation of icing experimental methods for further exploring the icing characteristics of rotary machines in the future.

2. Similarity Criterion of Icing Shape

The similarity criterion of icing shape used in the aeronautic field for translational motion models has four aspects: (1) similarity with respect to the flow field passing the body, (2) similarities with respect to droplet trajectory and impingement, (3) similarity with respect to water mass impinging a wall, and (4) similarities with respect to heat and mass transfer [17]. For the similarity criterion of icing shape for a rotating model, it is also necessary to consider the effect of rotation based on the above four aspects being satisfied. In other words, the similarity of icing on surfaces during rotation should be considered when the icing similarity criterion is applied under specific rotation conditions, such as the influence of centrifugal force or Coriolis force on icing.

Therefore, all of the above five aspects of similarity and their parameters were selected and defined in this paper.

2.1. Geometric Scaling Requirement. To test the icing shape similarity of a rotating model, the scale model should have a geometric profile identical to that of the full-scale model. Their characteristic lengths should be proportional, and the mounting angles, surface roughness, material properties, and other parameters should be the same.

For an airfoil model, the geometric similarity parameter is the chord length of the airfoil, and it is proportional between two models. It is defined by

$$c_m = kc_f, \tag{1}$$

where c_m is the chord length of the subscale model, c_f is the chord length of the full-scale model, and k is the ratio of the chord length of the full-scale model to that of the subscale model. Subscript m stands for the subscale model, and subscript f stands for the full-scale model.

2.2. Flow Field Scaling Requirement. According to the findings of previous researchers [16], when the flow velocity in the experiment is higher than that whose Reynolds number is 2.0×10^5, the principle of constant speed can be used. In such an instance, the flow velocities between the subscale model and full-scale model are the same. That is,

$$v_m = v_f, \tag{2}$$

where v_m is the wind velocity for the subscale model and v_f is the wind velocity for the full-scale model.

2.3. Droplet Trajectory and Impingement Scaling Requirement. To meet the similarity criterion of trajectory and impingement characteristics of water droplets colliding with the model surface, Langmuir et al. proposed an inertial correction parameter $\bar{K}$ [18]. It is defined by the following formulas:

$$\begin{aligned} \bar{K} &= \frac{K}{\mathrm{Re}_\infty^K}, \\ \bar{K} &= \left[\frac{\rho_\mathrm{d} R_\mathrm{a}^K}{18\mu_\mathrm{a}^{1-K}}\right] \frac{d_0^{2-K} U_\infty^{1-K} T^K}{L p^k}, \end{aligned} \tag{3}$$

where K is the inertial parameter, Re_∞ is the Reynolds number in the far field, ρ_d is the density of the droplets, R_a is the gas constant of air, μ_a is the viscosity coefficient of the air, d_0 is the diameter of the droplets, U_∞ is the velocity of the air, T is the temperature of the air, L is the characteristic length, and p is the pressure of the air.

To ensure that the subscale model has trajectories similar to those of the full-scale model, the inertial correction

parameters of the two models should be equal [12]:

$$\left(\bar{K}\right)_m = \left(\bar{K}\right)_f. \tag{4}$$

2.4. Mass of Water Droplet Impingement on the Wall Scaling Requirement. According to studies [16] on the similarity theory of icing on aircraft wings, the mass of water droplets impinging on the wall should satisfy the following formula:

$$\left(\frac{m_{\mathrm{i}}}{L}\right)_S = \left(\frac{m_{\mathrm{i}}}{L}\right)_R, \tag{5}$$

where m_{i} is the mass of icing and L is the characteristic length.

To simplify the similarity criterion of the mass of water droplets impinging on the wall, in this paper, a dimensionless parameter, the accumulation parameter A_c, is introduced based on the icing similarity theory. The parameter is defined by the following formula:

$$A_c = \frac{m_{\mathrm{i}}}{\rho_{\mathrm{ice}} L} = \frac{\mathrm{LWC} \bullet U_\infty \bullet t \bullet \beta}{\rho_{\mathrm{ice}} L}, \tag{6}$$

where ρ_{ice} is the density of ice, L is the characteristic length, LWC is the liquid water content, t is the icing time, and β is the water droplet collection rate.

According to formula (6), when the water droplet trajectories are similar and the experimental model and the full-scale model are strictly scaled, the density and the type of ice are the same.

Therefore, when the accumulation parameter is constant, as shown in formula (7), the icing mass generated by the impinging water droplet is similar.

$$(A_c)_m = (A_c)_f. \tag{7}$$

2.5. Thermodynamic Scaling Requirement. Icing on a rotating model involves phase change and heat mass transfer processes. To ensure that the icings on the full-scale model and the subscale model have the same type and characteristics, the thermodynamic characteristics on the surface of the full-scale model and the subscale model should be similar.

According to both the AEDC and ONERA criteria, the thermodynamic similarity of the icing process should meet the similarities of four parameters, which are defined and expressed as follows:

Freezing fraction n:

$$n = \frac{m_{\mathrm{i}}}{m_{\mathrm{w}}}, \tag{8}$$

where m_{i} is the mass of ice and m_{w} is the mass of water that impacts the surface of the blade.

Relative heat factor b:

$$b = \frac{m_{\mathrm{i}} C_{p,\mathrm{w}}}{h_c} = \frac{\mathrm{LWC} \bullet U_\infty \bullet \beta \bullet c_{p,\mathrm{w}}}{h_c}, \tag{9}$$

where $c_{p,\mathrm{w}}$ is the specific heat capacity of water at constant pressure, h_c is the heat transfer coefficient, β is the collection coefficient of water, m_{i} is the total mass of icing, m_{e} is the evaporation mass, m_{w} is the total mass of the water droplets impinging on the wall, h_c is the convective heat transfer coefficient, h_v is the heat of evaporation, and T_{sur} is the temperature of the model surface.

When formulating the icing similarity criterion under rime ice conditions, the freezing fraction is equal to 1. The temperature is an important condition to ensure that supercooled water droplets are frozen into rime ice. Therefore, when the icing shape similarity test is carried out under rime ice conditions, the test temperatures of two models with different sizes can be the same, but they must be low enough. That is,

$$T_s = T_f. \tag{10}$$

When the above conditions are met, the values of the freezing fractions of supercooled water droplets on model surfaces of different sizes are both equal to 1. This means that the freezing fractions are similar. Therefore, under this similarity, the relative heat factors b are also similar when the convective heat transfer coefficient h_c is the same. The droplet energy transfer driving potential ϕ is a function of parameters, such as the ambient temperature, the absolute temperature lower than 0°C, the incoming flow velocity, and the specific heat capacity of droplets. Similarly, the air energy transfer driving potential θ is a function of parameters, such as the ambient temperature, the model surface temperature, the incoming flow velocity, the heat of evaporation, and the evaporation mass. Therefore, the temperature of the model surface, the heat of water evaporation, and the evaporation mass are identical when the ambient temperatures are the same. Under conditions of similar flow fields over the body, the air energy transfer driving potential θ can also be similar.

2.6. Dynamic Pressure Scaling Requirements. The rotating model has the problem that ice generated on the surface can be shed. According to the studies by Xian on icing similarity [19], this problem can be solved by the relation between shear force and dynamic pressure. The shear force is proportional to the dynamic pressure. When the dynamic pressures of the two models are similar, the shear forces on both model surfaces are also similar. The expression of dynamic pressure is

$$q = \frac{1}{2} \rho_a V_\infty^2. \tag{11}$$

Substituting the ideal gas state equation into equation (11) gives

$$q = \frac{1}{2} \frac{m_a p}{nRT} V_\infty^2. \tag{12}$$

When the icing shapes are similar, the characteristics of ice shedding are also similar as the dynamic pressure is similar.

That is,

$$q_m = q_f. \tag{13}$$

2.7. Liquid Water Dynamic Scaling Requirement. To match the freezing fraction of the subscale model with that of the full-scale model, the surface liquid droplets of both models must have dynamic similarity. Therefore, it is necessary to match the ratio of the aerodynamic force to the surface tension of water droplets, that is, to match the Weber numbers. Kind and Potapczuk proposed a Weber number based on the thickness of water films, in which the density of air replaces that of water [20]. The results of this research show that the deviation of Weber numbers based on the water film thickness in icing similarity tests is not more than 25%. This indicates that the Weber number based on the water film thickness is an important parameter of the icing similarity theory. It is expressed by the following formula:

$$W_{e_w} = \frac{U_\infty^2 \delta_{w,A} \rho_a}{\sigma}. \tag{14}$$

When the Weber numbers based on water film thickness are matched, the relation between the subscale model and the full-scale model is as follows:

$$\left(W_{e_w}\right)_m = \left(W_{e_w}\right)_f. \tag{15}$$

2.8. Rotation Parameter Scaling Requirement. The difference in icing characteristics between rotating machines and aircraft wings is that the icing process of rotating machines, such as wind turbines, is also affected by rotation. Therefore, when formulating the icing similarity criterion for a rotating model, factors such as centrifugal force and Coriolis force should be considered [21]. In the formula of centrifugal force and Coriolis force, there are only three parameters: mass, rotating angular speed, and rotating radius. Consequently, centrifugal force is selected as a rotating parameter to formulate the similarity criterion. In this paper, the ratio of centrifugal force to surface area is defined as a rotating similarity parameter called "centrifugal tensile stress." It is expressed by the following formula:

$$\sigma_c = \frac{m\omega^2 r}{S_{\text{cov}}}, \tag{16}$$

where S_{cov} is the area of blade covered by ice.

As a result, the subscale model and the full-scale model shall have similar centrifugal tensile stresses:

$$(\sigma_c)_m = (\sigma_c)_f. \tag{17}$$

2.9. Selection Principles of Experimental Parameters. The icing similarity criterion under rotating and rime ice conditions was deduced in this paper. Specifically, the similarity criterion was formulated by the modified inertia parameter, the accumulation parameter, the freezing fraction, the relative heat factor, the air energy transfer driving potential, the droplet energy transfer driving potential, the Weber number based on water film thickness, and the centrifugal tensile stress. The selection sequence of the icing similarity parameters under rime ice conditions for a rotating model is determined as follows:

(1) Characteristic length of the subscale model:

$$c_m = kc_f. \tag{18}$$

(2) Wind speed in the test of the subscale model:

$$v_m = v_f. \tag{19}$$

(3) Test temperature:

$$T_m = T_f. \tag{20}$$

(4) Diameter of water droplet:

$$d_m = \left(\frac{c_m}{c_f}\right)^{1/(2-\kappa)} \left(\frac{p_m}{p_f}\right)^{\kappa/(2-\kappa)} \left(\frac{T_m}{T_f}\right)^{-\kappa/(2-\kappa)} \left(\frac{v_m}{v_f}\right)^{(\kappa-1)/(2-\kappa)} d_f. \tag{21}$$

(5) Liquid water content (LWC):

$$(\text{LWC})_m = (\text{LWC})_f \left(\frac{v_m}{v_f}\right)^3 \left(\frac{(d_0)_m}{(d_0)_f}\right) \left(\frac{(\rho_a)_m}{(\rho_a)_f}\right). \tag{22}$$

(6) Test pressure:

$$P_m = P_f \left(\frac{v_m}{v_f}\right) \left(\frac{T_m}{T_f}\right)^2. \tag{23}$$

(7) Test time:

$$t_m = t_f \left(\frac{c_m}{c_f}\right)\left(\frac{v_m}{v_f}\right)^{-1}\left(\frac{\mathrm{LWC}_m}{\mathrm{LWC}_f}\right)^{-1}. \quad (24)$$

(8) Rotating angular velocity:

$$\omega_m = \omega_f \left(\frac{\beta_f}{\beta_m}\right)^{0.5}\left(\frac{\mathrm{LWC}_f}{\mathrm{LWC}_m}\right)^{0.5}\left(\frac{C_f}{C_m}\right)^{0.5}\left(\frac{t_f}{t_m}\right)^{0.5}\left(\frac{r_f}{r_m}\right)^{0.5}\left(\frac{(S_{\mathrm{cov}})_m}{(S_{\mathrm{cov}})_f}\right)^{0.5}. \quad (25)$$

3. Experimental System and Scheme

3.1. Experimental System. In this paper, a self-developed icing wind tunnel system was utilized to conduct the icing test on a rotating model, as shown in Figure 1. Images of the test system are shown in Figure 2. Wind tunnels were rebuilt on the basis of existing low-speed aerodynamic wind tunnels. A stable cooling environment could be achieved by connecting the wind tunnel entrance section to the outdoors based on the natural low-temperature climate in Northeast China. A two-phase flow spray system was added to the outlet of the airway. The spray section consisted of a microspray nozzle from Tanaka, Japan, in which the spray volume was 0.5~12.4 l/h and the droplet size was 20~100 μm. The model icing test was completed in the test section when the water droplets and cold air were fully mixed in the mixing section. The rotating system drove the model to rotate and complete icing in the test section. Due to wind tunnel size limitations, the radius of rotation could not be very long; it is necessary to increase either the wind speed or the model rotating speed. This situation posed a challenge to the system, so the structure of the traditional test section was further optimized. The test section is comprised of a spray zone and a nonspray zone. The axis of the rotating model is located at the nonspray zone. When the model rotates into the spray zone, ice is frozen on the model surface. In this system, the rotating radius of the sample can be adjusted, and the rotating center is aligned with the center of the cross section of the wind tunnel. The motion diagram of the rotating model in the icing wind tunnel is shown in Figure 3. This method can reduce the size of the icing in the wind tunnel as well as the cost of the experimental system. In the test process, due to many environmental factors, the natural environment was monitored over time to ensure that the temperature change of the natural environment was less than 1°C during the testing period. The spray system was initially calibrated, its spray characteristics were optimized, and the spray volume was also calibrated before each test. Throughout the test, the whole duct was fully precooled. The thermocouple installed in the nonspray section ensured that the duct remained below 0°C, and the uniformity of the spray position was calibrated to ensure that the LWC and MVD in each system test are consistent. In this paper, each test was carried out under the condition of stable external temperature. After many tests, the results showed that the parameters of the test system were stable. The average deviation of temperature in the duct was ±0.5°C, the average deviation of wind speed was ±0.1 m/s, the turbulence degree of the wind tunnel was 0.04%, the average deviation of LWC was ±0.02 g/m^3, and the average deviation of MVD was ±2 μm [22]. Each test result was repeated 2~3 times for real-time recording with a CCD camera to ensure reproducibility.

The test model was exposed to icing in the tunnel at a ninth of the circular trajectory. Then, eight-ninth of its trajectory was exposed to the nonspray section. We verified that the icing trend did not change, and the experimental parameters for the original test system were determined. The experimental parameters for the new test system were selected and calculated as follows: (1) characteristic length d_m was 20 and 40 mm, (2) wind velocity v_f was 10 m/s, (3) experimental temperature T_f was -15°C, (4) experimental environment pressure P_f was 101325 Pa, (5) medium volume diameter $(\mathrm{MVD})_f$ was 50 μm, (6) liquid water content $(\mathrm{LWC})_f$ was 0.58 g/m^3, (7) test time length t_f was 68.3 min, (8) rotating radius r_f was 0.45 m, and (9) rotating velocity n_f was 333 r/min. The results are shown in Figure 4. The ice shape trends of the two systems were roughly the same, and the ice shapes were highly consistent. This shows that the new system does not change the icing trend.

3.2. Experimental Scheme. Based on the traditional icing test method in the aviation field, a solid aluminum cylinder was selected as the experimental object in this paper. The icing process is a physical and complex process with heat mass transfer. To decrease the influence of the thermal conductivity of the material on the test, aluminum was selected as the material because of its good thermal conductivity, high stiffness, and high hardness. In this paper, two sizes of cylinder samples were selected with diameters of 20 mm and 40 mm. The heights of both samples were 20 mm, and their roughness was 3.2 μm. Schematic diagrams of the 3D models and samples are shown in Figures 5 and 6, respectively.

In this paper, a cylinder with a diameter of 40 mm was selected as the full-scale sample, while a cylinder with a diameter of 20 mm was selected as the subscale sample. To validate the accuracy of the icing shape similarity criterion for the rotating model proposed in this study under rime ice conditions, an experimental scheme was designed according to the above selection order and test parameter principles. The experimental scheme is provided in Table 1.

As shown in Table 1, case 1, case 3, and case 5 are the experimental conditions for the subscale sample; case 2, case 4, and case 6 are the experimental conditions for the full-scale sample.

These two sample groups have the following corresponding scale relations: the sample in case 1 is the subscale model that corresponds to the full-scale model in case 2, the sample in case 3 is the subscale model that corresponds to the full-scale model in case 4, and the sample in case 5 is the subscale model that corresponds to the full-scale model in case 6. Each scheme selects 6 time lengths for the icing test to investigate the effect of time on the icing shape similarity under rime ice conditions. For example, the process of selecting the experimental

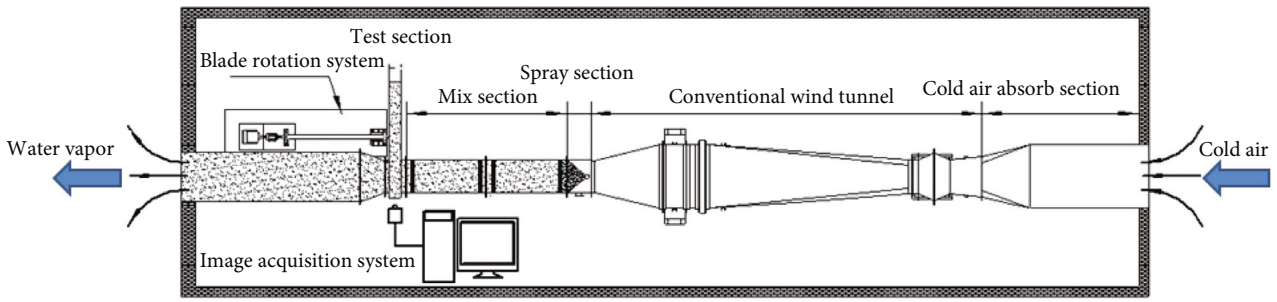

Figure 1: Schematic diagram of the icing wind tunnel test system.

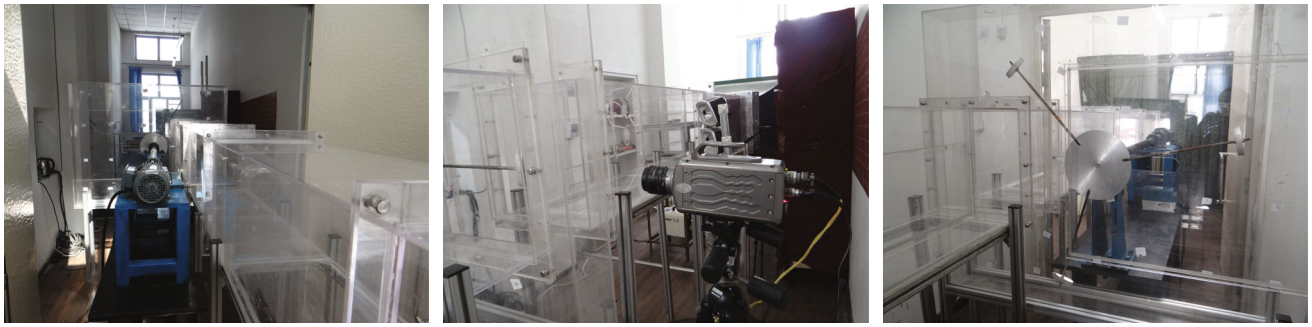

Figure 2: Images of the test system.

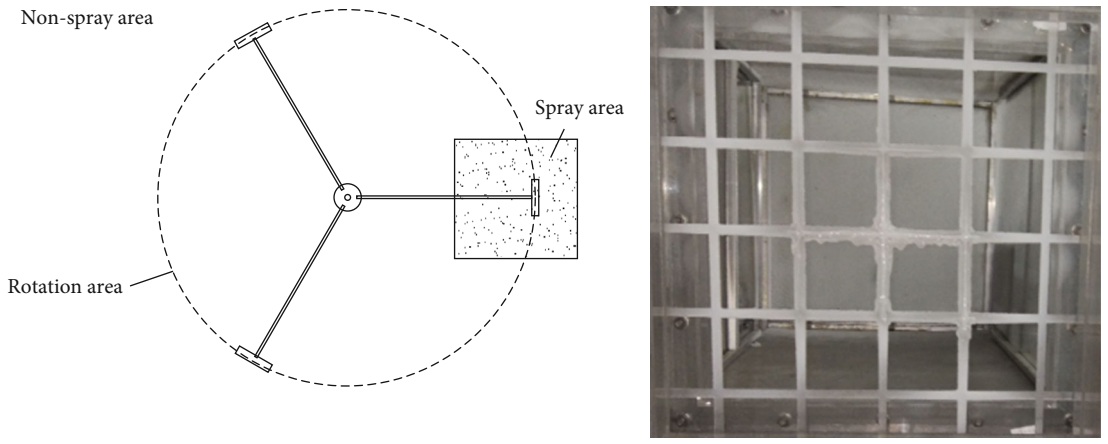

Figure 3: Schematic diagram and ice grid of the test system.

parameters based on the icing shape similarity criterion in cases 1 and 2 is explained as follows.

The experimental parameters for the full-scale sample were decided, and these parameters are listed as follows: (1) characteristic length d_f was 40 mm, (2) experimental wind velocity v_f was 10 m/s, (3) experimental temperature T_f was -15°C, (4) experimental environment pressure P_f was 101325 Pa, (5) medium volume diameter $(\mathrm{MVD})_f$ was 50 μm, (6) liquid water content $(\mathrm{LWC})_f$ was 0.58 g/m^3, (7) test time t_f was 12 min, (8) rotating radius r_f was 0.5 m, (9) and rotating velocity n_f was 400 r/min.

According to the selection principle of the experimental parameters of the icing shape similarity criterion, the experimental parameters of the subscale sample were selected and calculated as follows: (1) characteristic length d_m was 20 mm; (2) subscale ratio κ was 1/2; (3) experimental wind velocity v_m was 10 m/s, which was the same as v_f; (4) experimental temperature T_m was -15°C; (5) experimental environment pressure P_m was 101325 Pa, which was calculated by formula (23); (6) medium volume diameter $(\mathrm{MVD})_m$ was 50 μm, which was calculated by formula (21); (7) liquid water content $(\mathrm{LWC})_m$ was 0.58 g/m^3, which was calculated by formula (22); (8) test time t_m was 6 min, which was

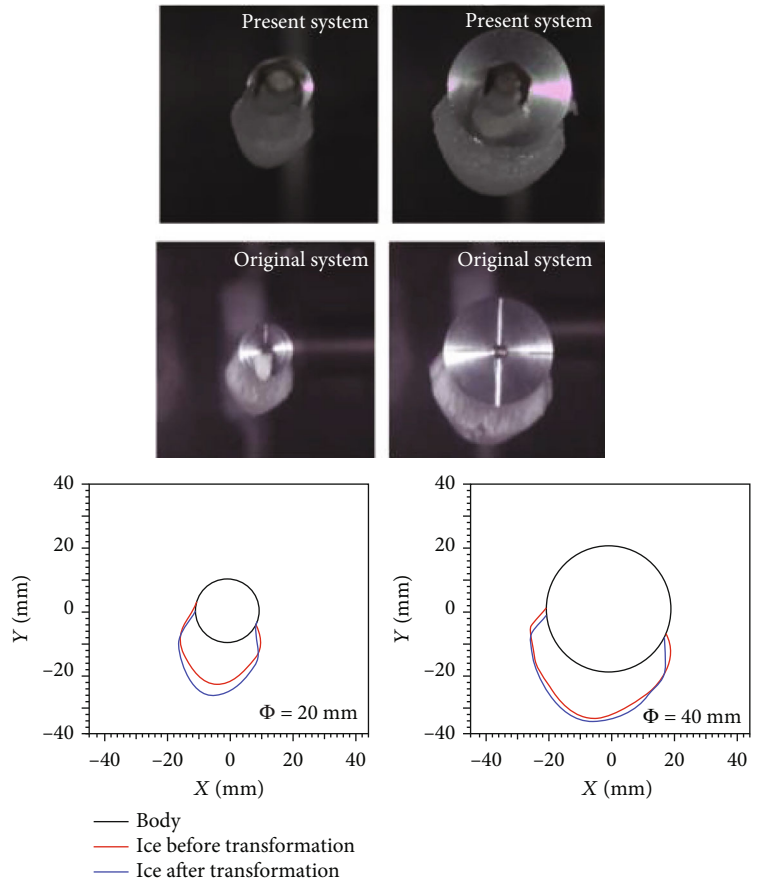

Figure 4: Comparison of cylinder icing.

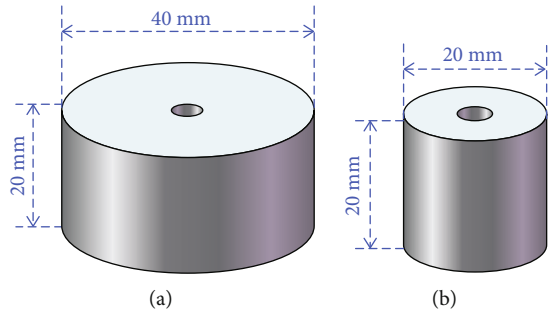

Figure 5: 3D model cylinder: (a) $\phi = 40$ mm cylinder; (b) $\phi = 20$ mm cylinder.

calculated by formula (24); (9) rotating radius r_m was 0.5 m; and (10) rotating velocity n_m was 200 r/min, which was calculated by formula (25).

4. Results and Discussion

4.1. Experimental Results. The distributions and shapes of icing on the surfaces of rotating cylinders of different sizes are shown in Figure 7. As shown in Figure 7(a), the icing shapes at different cross sections of the icing cylinder are approximately the same. Therefore, the icing shape at the end of the cylinder was selected as the research object instead of the icing shape on the whole rotating cylinder surface, and it was used to analyze the distribution and shape of icing on the surface of the rotating cylinder, as shown in Figure 7(b).

The images of icing distributions on the cylinder surface under different experimental conditions were captured by a high-speed camera and are shown in Figure 8.

As seen in Figure 8 under three contrast conditions, the icing shapes on the surfaces of full-scale cylinders are approximately the same as those on the surfaces of subscale cylinders and have good similarities. According to the experimental results, the icing shapes grow layer-by-layer over time. The amount of icing is directly proportional to the length of time. When the rotation speed is 400 r/min, the icing shapes of the full-scale samples and subscale samples

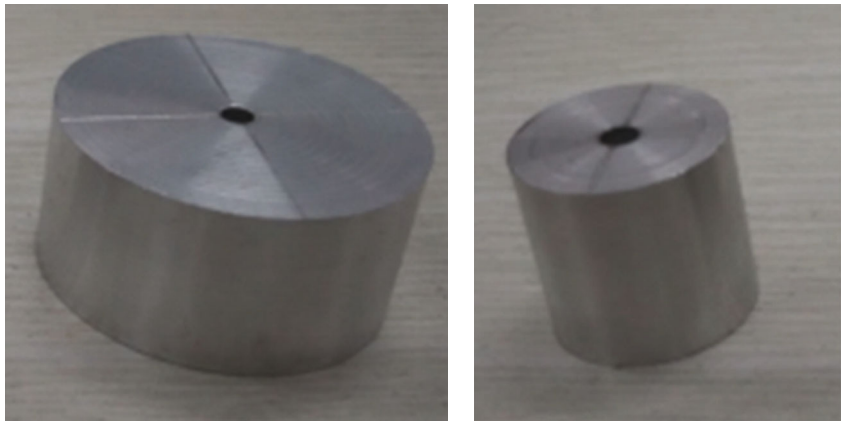

(a) (b)

Figure 6: Cylinder sample: (a) $\phi = 20$ mm cylinder; (b) $\phi = 40$ mm cylinder.

Table 1: Experimental scheme.

Contrast condition	Case	v (m·s^{-1})	T (°C)	MVD (μm)	LWC (g·m^{-3})	P (Pa)	n (rpm)	d (mm)	Time (s)					
									t_1	t_2	t_3	t_4	t_5	t_6
C1	No. 1	10	-15	50	0.58	1×10^6	400	20	6	12	18	24	30	36
	No. 2						400	40	12	24	36	48	60	72
C2	No. 3						800	20	6	12	18	24	30	36
	No. 4						800	40	12	24	36	48	60	72
C3	No. 5						1200	20	6	12	18	24	30	36
	No. 6						1200	40	12	24	36	48	60	72

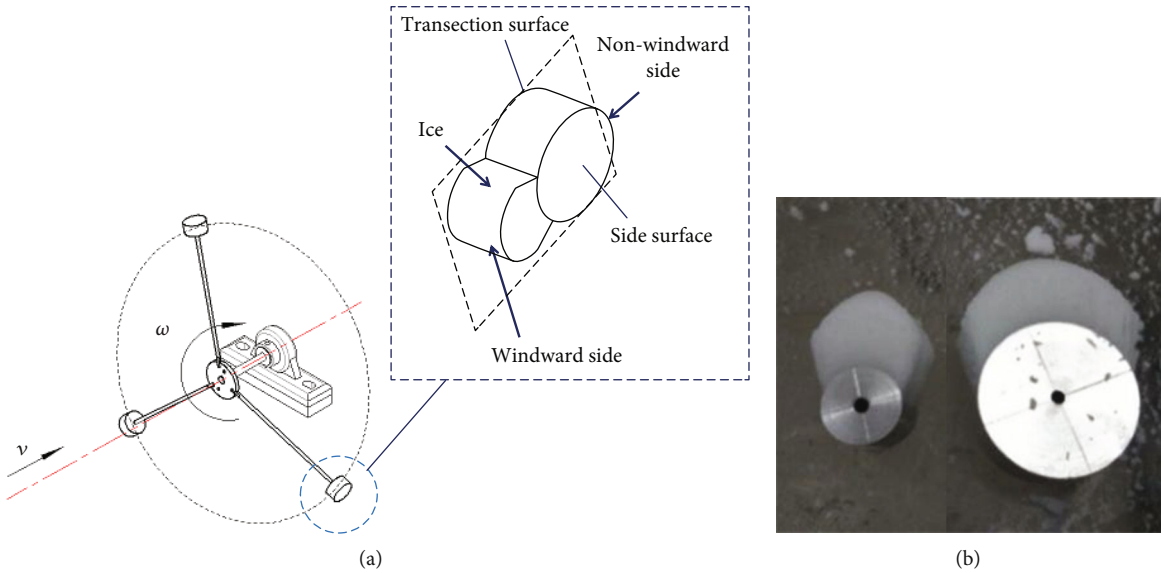

(a) (b)

Figure 7: Icing distributions on surfaces of rotating cylinders: (a) schematic diagram of the rotating cylinder; (b) distributions of icing on the cylinder.

are both approximately circular arcs at the initial stage of icing. Subsequently, the icing shape changes to an elliptical arc with increasing icing time. When the rotation speed is 800 r/min or 1200 r/min, the icing shapes on the full-scale and subscale sample surfaces all display bulge-like shapes with circular arcs at the initial icing stage, and these bulge arcs change to straight lines with increasing icing time.

According to the experimental results in Figure 8, not all upwind surfaces of the cylinders are covered by ice layers, and the scope of icing has a downward movement with increasing rotation speed. In contrast, the scope of icing on the downwind surfaces of the cylinders shows an upward movement. The reason for this trend is that the relative wind speed, which is the resultant velocity of the rotating speed

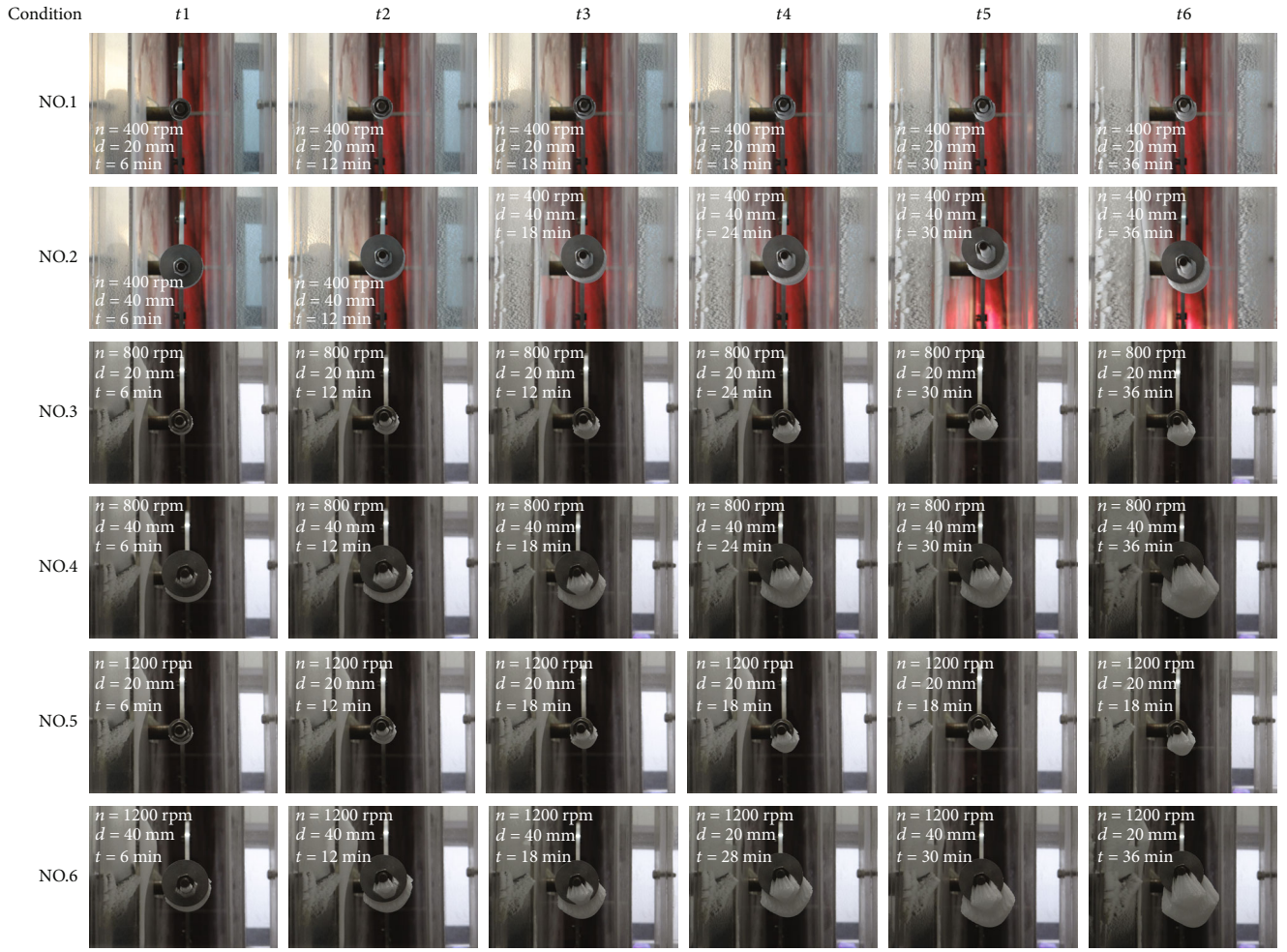

Figure 8: Images of icing distributions on surfaces of cylinders with different sizes.

and wind speed, changes and influences the position and scope of icing on the cylinder surface. The relative wind speed is one of the important factors that influences icing shape and distribution. Detailed research on this issue was carried out in the previous paper [23].

As shown in Figure 9, the icing distribution and shapes on the different sizes of cylinders are approximately the same. The location of the starting point and the changing trend of the icing shapes are consistent. These research results validate the correctness of the icing shape similarity criterion for the rotating models proposed in this paper under rime ice conditions.

4.2. Evaluation of Icing Shape Similarity. To quantitatively analyze the icing shapes on different sizes of cylinders, a method for evaluating the similarity of irregular icing shapes on cylinders with different scales was defined based on the previous work [15]. This method was based on five typical characteristics of icing shape, including icing area S, thickness of icing stagnation point σ, deflection angle of icing stagnation point α, superior limit of icing L_{u} and inferior limit of icing L_{d}, as shown in Figure 10.

Because the sizes of cylinders are different, the benchmarks for comparatively analyzing the typical characteristics of icing shapes on different sizes of cylinders are inconsistent. Therefore, several dimensionless parameters are defined as follows in this paper.

Dimensionless icing area η_s:

$$\eta_s = \frac{S}{\pi(d/2)^2}, \tag{26}$$

where d is the diameter of the cylinder.

Dimensionless thickness of icing stagnation point η_σ:

$$\eta_\sigma = \frac{\sigma}{d}. \tag{27}$$

Dimensionless superior limit of icing L_{u}:

$$\eta_{L_{\mathrm{u}}} = \frac{L_{\mathrm{u}}}{d}. \tag{28}$$

Dimensionless inferior limit of icing L_d:

$$\eta_{L_{\mathrm{d}}} = \frac{L_{\mathrm{d}}}{d}. \tag{29}$$

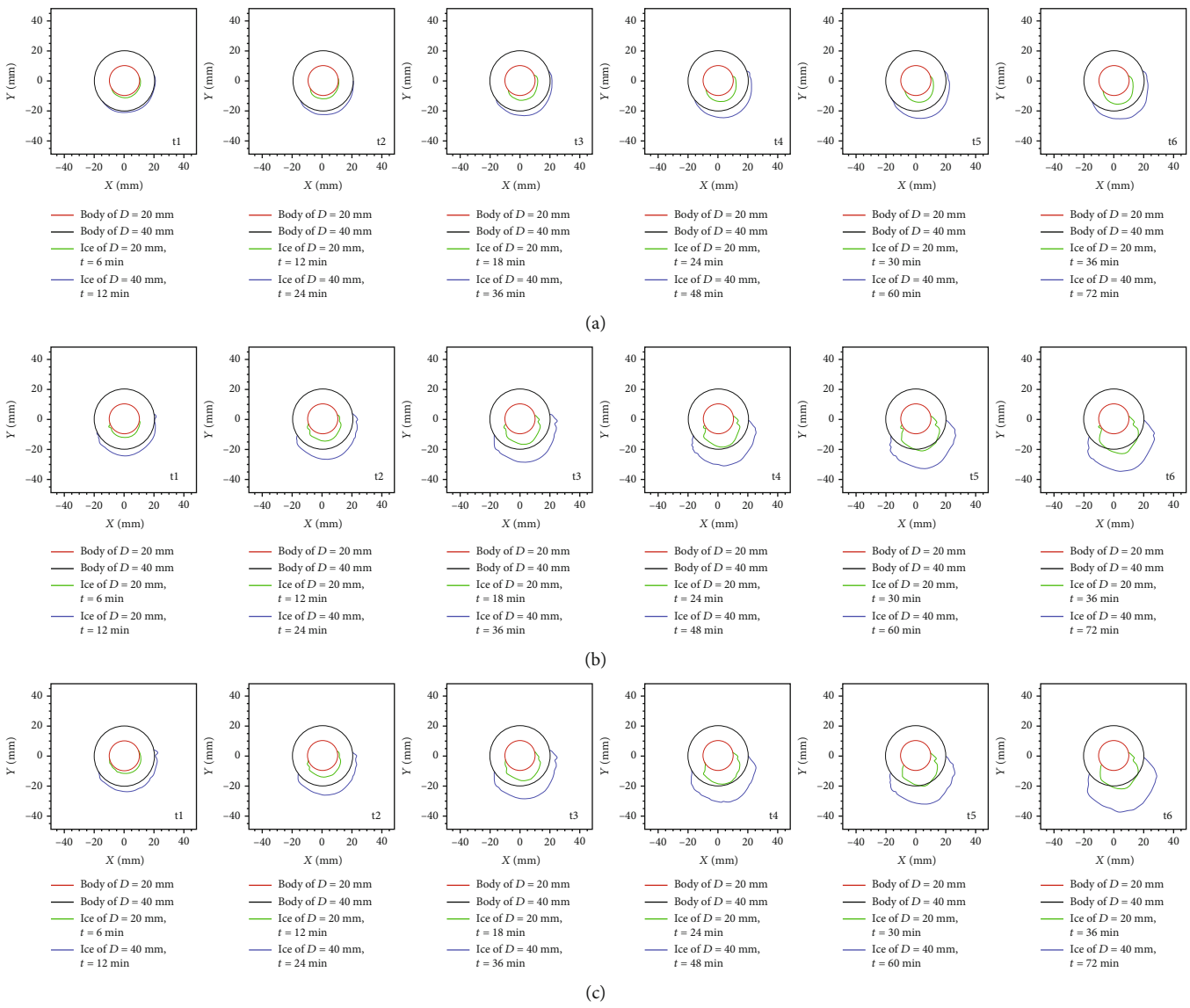

Figure 9: Icing shapes on surfaces of different sizes of cylinders in the same coordinate system with the same scale: (a) comparison of icing shapes between conditions no. 1 and no. 2; (b) comparison of icing shapes between conditions no. 3 and no. 4; (c) comparison of icing shapes between conditions no. 5 and no. 6.

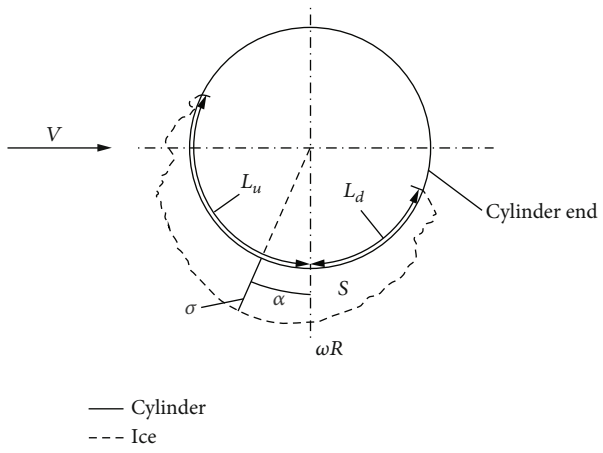

Figure 10: Typical characteristics of icing shape on the cylinder.

The comparative results of dimensionless icing areas on different sizes of cylinders are shown in Figure 11.

As shown in Figure 11, the changing trends of the dimensionless icing areas on cylinder surfaces of different sizes are almost the same with increasing icing time. The growth trends are approximately directly proportional to the time of the icing test. In the same icing period, the dimensionless icing area under 400 r/min conditions is the smallest. The reason for this result is that the cylinder can collect more supercooled droplets per unit time with increasing rotation speed. In addition, the dimensionless icing areas are nearly equal in the same icing period under 800 r/min and 1200 r/min conditions.

The comparative results of the dimensionless thickness of the icing stagnation point in different sizes of cylinders are shown in Figure 12.

As shown in Figure 12, the coincidence ratio of the curves between the dimensionless thicknesses of the icing

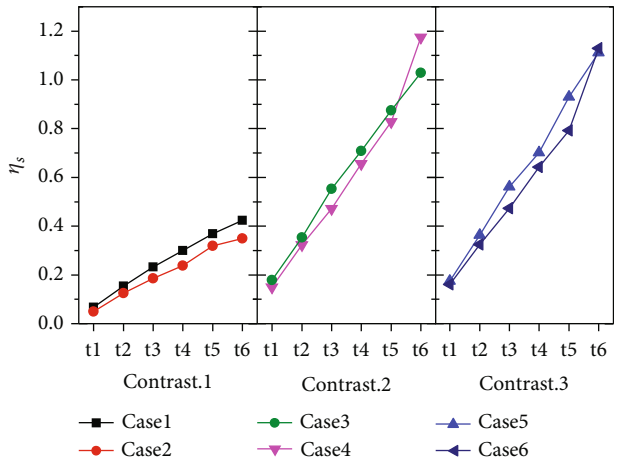

Figure 11: Comparative results of dimensionless icing areas.

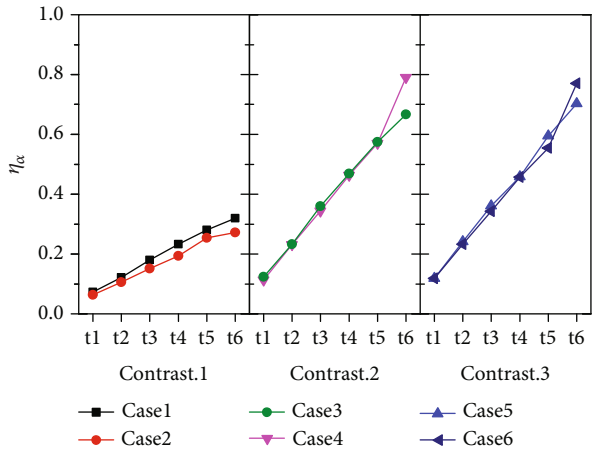

Figure 12: Comparative results of the dimensionless thickness of the icing stagnation point.

stagnation point on cylinders of different sizes is high. The growth trend is similar to that of the dimensionless icing area. The dimensionless thickness of the stagnation points increases with rotation speed. When the rotation speed is higher than 800 r/min, the dimensionless thickness of the icing stagnation point shows little difference in the same icing period under different rotation speeds. The reason for this result is that the droplet collection coefficient of the icing cylindrical surface reaches a limit with increasing rotation speed.

The comparative results of the dimensionless icing superior limit and inferior limit for cylinders of different sizes are shown in Figures 13 and 14, respectively. Here, the dimensionless icing limit curves for cylinders of different sizes have obvious discrepancies. The reason for this result is that the experiments with cylinders of different sizes have the same MVD, and the MVD is a key factor that determines the location of icing on the object surface. However, this has little effect on the icing area and other dimensionless parameters. This leads to the discrepancies in the icing limit of cylinder surfaces with different sizes.

The comparative results of the deflection angles of icing stagnation points on cylinder surfaces with different sizes are shown in Figure 15.

As shown in Figure 15, the deflection angles of icing stagnation points on icing cylinders at both scales distinctly fluctuate with increasing test times, but they ultimately tend to coincide. The reason for this result is that the thickness of the icing layer grows with increasing icing time, and the process of icing, which involves heat and mass transfer that is influenced by the temperature of the cylinder surface, becomes weaker. The processes of heat and mass transfer between the droplet and ice layer greatly influence the process of icing. When the experimental conditions are the same, the characteristics of heat and mass transfer between the ice layer and the droplet are also the same for cylinders of different sizes.

Based on the above analysis, there are discrepancies in the typical characteristics of icing shapes for the cylinder surfaces of different sizes. To analyze these discrepancies, some characteristic parameters, which are utilized to quantify the discrepancy in icing shape, are defined based on the 5 typical icing characteristics mentioned above. The definitions and expressions of these parameters are listed as follows [22]:

Dimensionless icing area discrepancy rate ς_S:

$$\varsigma_S = \left| \frac{(\eta_S)_p - (\eta_S)_m}{(\eta_S)_p} \right|. \tag{30}$$

Dimensionless thickness of icing stagnation point discrepancy rate ς_σ:

$$\varsigma_\sigma = \left| \frac{(\eta_\sigma)_p - (\eta_\sigma)_m}{(\eta_\sigma)_p} \right|. \tag{31}$$

Dimensionless icing superior limit discrepancy rate ς_{L_u}:

$$\varsigma_{L_u} = \left| \frac{\left(\eta_{L_u}\right)_p - \left(\eta_{L_u}\right)_m}{\left(\eta_{L_u}\right)_p} \right|. \tag{32}$$

Dimensionless icing inferior limit discrepancy rate ς_{L_d}:

$$\varsigma_{L_d} = \left| \frac{\left(\eta_{L_d}\right)_p - \left(\eta_{L_d}\right)_m}{\left(\eta_{L_d}\right)_p} \right|. \tag{33}$$

Dimensionless deflection angle of icing stagnation point discrepancy rate ς_α:

$$\varsigma_\alpha = \left| \frac{(\eta_\alpha)_p - (\eta_\alpha)_m}{(\eta_\alpha)_p} \right|. \tag{34}$$

where the parameters with subscript p belong to the full-scale model and those with subscript m belong to the subscale model.

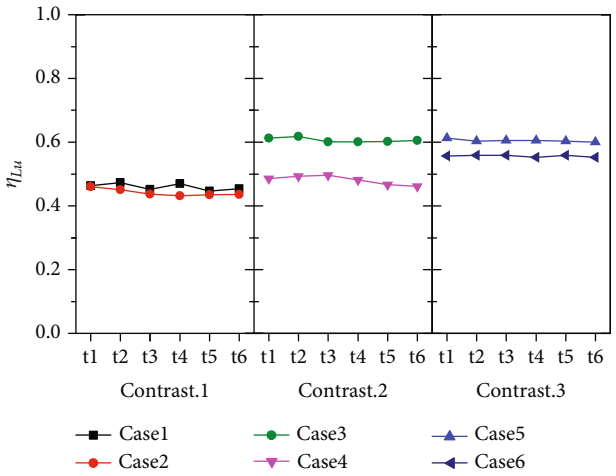

Figure 13: Comparative results of dimensionless icing superior limits.

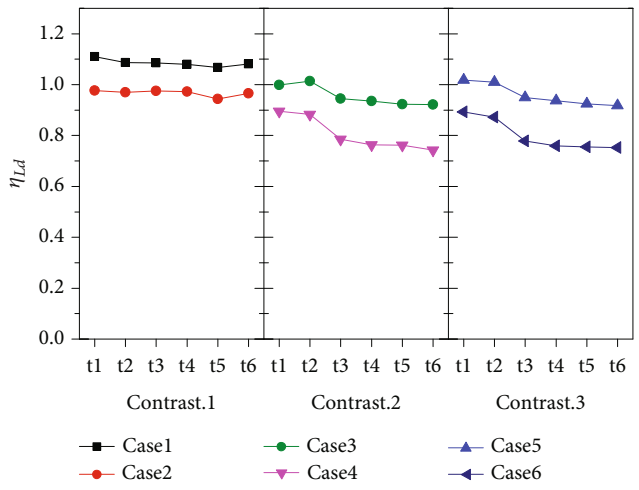

Figure 14: Comparative results of dimensionless icing inferior limits.

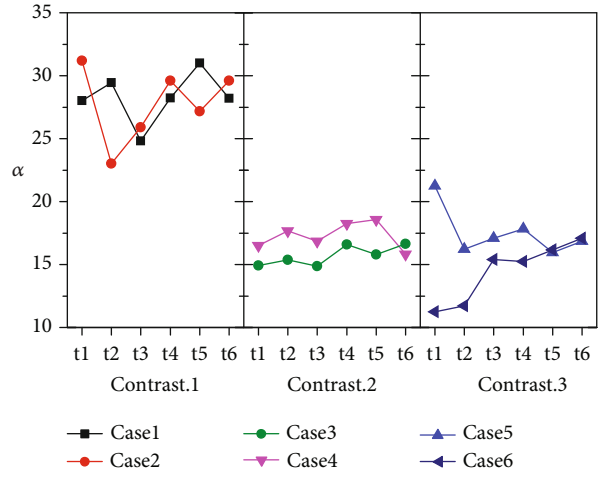

Figure 15: Comparative results of the deflection angle of the icing stagnation point.

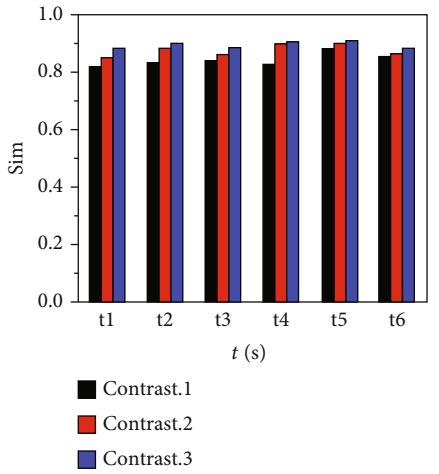

Figure 16: Icing similarity rate under different working conditions.

For assessing similarity, the degree of influence of each characteristic should also be considered. Based on previous work, weighting factors are given to different characteristics, and their values are 0.3 (r_σ), 0.3 (r_S), 0.1 (r_α), 0.15 (r_{L_u}), and 0.15 (r_{L_d}).

According to the previous work [18], the icing area and thickness of the icing stagnation point are key factors for evaluating the icing shape. The icing superior and inferior limits have little influence. To quantitatively analyze the similarity of icing shapes, the parameter "icing similarity rate" is defined and expressed in this paper as follows.

$$\mathrm{Sim} = \left[1 - \left(r_\sigma \varsigma_\sigma + r_S \varsigma_S + r_\alpha \varsigma_\alpha + r_{L_u} \varsigma_{L_u} + r_{L_d} \varsigma_{L_d}\right)\right], \quad (35)$$

where Sim is the icing similarity rate.

The icing shape similarity criterion and the evaluation method proposed in this paper are used to quantitatively analyze the icing shapes on two sizes of cylinder surfaces under different experimental conditions. The dimensionless icing area, the dimensionless thickness of the icing stagnation point, the dimensionless icing superior and inferior limits, and the dimensionless deflection angle of the icing stagnation point are substituted into formula (35). The resulting bar chart of icing similarity rates is shown in Figure 16.

As shown in Figure 16, the icing time has little influence on the icing similarity rate. Under the same experimental conditions, the icing similarity rates for two cylinders of different sizes change slightly with increasing icing time. When the icing time is the same, the higher the rotation speed is, the higher the icing shape similarity rate is. The similarity rate under the contrast 3 condition reaches 91%. The reason for this result is that when LWC and MVD are constant, the unit surface areas of the cylinders of different sizes collect the same amount of droplets per unit time, and the capacity for collecting droplets increases with increasing rotation speed until the maximum limit is reached. This factor leads to the increase in the icing similarity rate with the increase in rotation speed. For the special case of t_5, the Sim of contrast 2 was lower than that of contrast 1 and contrast 2. The reason for this result may

Table 2: Similarity rate of different conditions.

Contrast condition	Case	v (m·s^{-1})	T (°C)	MVD (μm)	LWC (g·m^{-3})	P (Pa)	n (rpm)	d (mm)	Sim (%)					
									t_1	t_2	t_3	t_4	t_5	t_6
C1	No. 1	10	-15	50	0.58	1×10^6	400	20	81	83	84	82	88	83
	No. 2						400	40						
C2	No. 3						800	20	85	88	85	89	89	85
	No. 4						800	40						
C3	No. 5						1200	20	87	89	87	90	90	86
	No. 6						1200	40						

be related to the abnormal fluctuation of wind speed and turbulence in the wind tunnel within such a small range, or the nozzle in the spray system may have some problems. However, this single result does not affect the overall results of the test because in looking at the overall effect of the test, the laws of other working conditions are the same (except t_5, where the similarity rates are as follows: contrast 1 is less than contrast 2, which is less than contrast 3). Therefore, this very special phenomenon does not affect the overall conclusion of the experiment. By quantitatively analyzing the icing shape similarity rate with different sizes, the accuracy of the icing shape similarity criterion proposed in this paper is validated. The results lay the foundations for icing similarity tests of rotating parts, such as wind turbine blades, in icing wind tunnels.

5. Conclusions

In this paper, studies on the icing shape similarity on a rotating cylinder were carried out, and three conclusions are summarized as follows:

(1) A novel icing shape similarity criterion was established. The parameter "centrifugal tensile stress" was proposed and defined as an icing similarity parameter for evaluating the similarity of the rotating model. The icing shape similarity criterion for the rotating model under rime ice conditions was subsequently formulated based on the Weber number of the water film thickness. The primary principle and sequence of experimental parameter selection were determined

(2) Experimental studies on the icing shape similarity criterion for the rotating model under rime icing conditions were carried out based on cylinders of two different sizes. The experimental results show that icing shapes on cylindrical surfaces of two different sizes under different working conditions had high similarities. The location of icing, the icing shape, and the trend of changes in icing with increasing time had high consistency

(3) Several dimensionless parameters and discrepancy rates were defined to characterize the similarity of icing shapes. The dimensionless icing areas were approximately directly proportional to the test time. The dimensionless thicknesses of icing stagnation points on cylinders of different sizes had high coincidence and little difference when the rotation speed was high. The deflection angles of the icing stagnation points at both scales tended to coincide as the test time increased. As shown in Table 2, the similarity rate ranged from 81% to 90%.

This study carried out a prospective study only for the specific conditions of rime ice, which is also a common idea in the field of aviation icing research. However, in this paper, icing similarity research based on cylinders was carried out, though its aerodynamic performance is obviously different from that of airfoils. The icing similarity of airfoils requires further exploration and demonstration, and more research work will be carried out.

Nomenclature

c: Chord length (m)
b: Blade
D: Rotor diameter (m)
E: Energy (J)
f: Full-scale model
L: Icing limit (mm)
LWC: Liquid water content (g/m^3)
MVD: Medium volume droplet diameter (μm)
m: Subscale model
Q: Quantity of heat (J)
U: Velocity of wind flows (m/s)
Sim: Similar degree (%)
r_i: Weighting factor
η: Dimensionless method
δ_S: Stationary point thickness (mm)
L_d: Downer impingement limit
L_u: Upper impingement limit
v: Peripheral speed (m/s)
α_s: Deflection angle of icing
θ: Rotation angle of airfoil (°)
cov: Cover
S_{cov}: Icing area (mm^2)
t: Icing time (s)
T: Temperature (°C)
ς: Difference rate factor.

Data Availability

The data used to support the findings of this study are included within the article.

Conflicts of Interest

The authors declare that there are no conflicts of interest regarding the publication of this paper.

Acknowledgments

This research is supported by the National Natural Science Foundation of China (NSFC, Nos. 51976029 and 51576037).

References

[1] Y. Li, K. Tagawa, F. Feng, Q. Li, and Q. He, "A wind tunnel experimental study of icing on wind turbine blade airfoil," *Energy Conversion and Management*, vol. 85, pp. 591–595, 2014.

[2] M. M. Peiravi, J. Alinejad, D. D. Ganji, and S. Maddah, "Numerical study of fins arrangement and nanofluids effects on three-dimensional natural convection in the cubical enclosure," *Challenges in Nano and Micro Scale Science and Technology*, vol. 7, no. 2, pp. 97–112, 2019.

[3] M. M. Peiravi, J. Alinejad, D. D. Ganji, and S. Maddah, "3D optimization of baffle arrangement in a multi-phase nanofluid natural convection based on numerical simulation," *International Journal of Numerical Methods for Heat & Fluid Flow*, vol. 30, no. 5, pp. 2583–2605, 2020.

[4] ISO E, *Atmospheric icing of structures*, no. article 12494, 2001International Standard: ISO, 2001.

[5] L. Ville, "Available technologies of wind energy in cold climates," *IEA Wind Task*, vol. 19, 2016.

[6] G. L. Taylor, *Notes on possible equipment and technique for experiments on icing on aircraft*, HM Stationery Office, 1940.

[7] J. Shin and T. Bond, "Results of an icing test on a NACA 0012 airfoil in the NASA Lewis Icing Research Tunnel," in *30th Aerospace Sciences Meeting and Exhibit Reno*, NV, USA, 1992.

[8] M. C. Homola, M. S. Virk, and T. Wallenius, "Effect of atmospheric temperature and droplet size variation on ice accretion of wind turbine blades," *Journal of Wind Engineering and Industrial Aerodynamics*, vol. 98, no. 12, pp. 724–729, 2010.

[9] R. Flemming, P. Alldridge, and R. Doeppner, "Artificial icing tests of the S-92A helicopter in the McKinley climatic laboratory," in *AIAA Aerospace Sciences Meeting & Exhibit*, Texas, USA, 2013.

[10] T. Wei, O. Ahmet, and H. Hui, "A wind tunnel study of wind loads on a model wind turbine in atmospheric boundary layer winds," *Journal of Fluids and Structures*, vol. 85, pp. 17–26, 2019.

[11] Y. Li, S. Wang, Q. Liu, F. Feng, and K. Tagawa, "Characteristics of ice accretions on blade of the straight-bladed vertical axis wind turbine rotating at low tip speed ratio," *Cold Regions Science and Technology*, vol. 145, no. 13, pp. 1229–1236, 2018.

[12] H. Yiqiang, P. Jose, and S. Sven, "Scaled ice accretion experiments on a rotating wind turbine blade," *Journal of Wind Engineering & Industrial Aerodynamics*, vol. 109, pp. 55–67, 2012.

[13] E. H. Kuohsing, T. V. Giao, and S. B. Colin, *Water droplet impingement on simulated glaze, mixed, and rime ice accretions*, 2007, NASA TM-2007-213961.

[14] E. T. Jackson, *Development study: the use of scale models in an icing tunnel to determine the ice catch on a prototype aircraft with particular reference to Concorde*, SST/B75T/TMMcK/242. British Aircraft Corp. (Operating) Ltd., Filton Division, 1967.

[15] G. A. Ruff, "Quantitative comparison of ice accretion shapes on airfoils," *Journal of Aircraft*, vol. 39, no. 3, pp. 418–426, 2002.

[16] G. A. Ruff, *Analysis and verification of the icing scaling equations*, vol. 1, 1986AEDC-TR-85-30.

[17] A. J. Bilanin, "Proposed modifications to the ice accretion/icing scaling theory," *Icing Scaling Theory*, 1988, AIAA Paper AIAA-88-0203.

[18] I. Langmuir, "A mathematical investigation of water droplet trajectories," *Army Air Forces Technical Report No. 5418*, 1946.

[19] X. Yi, *Numerical Computation of Aircraft Icing and Study on Icing Test Scaling Law*, China Aerodynamics Research and Development Center, 2007, (in Chinese).

[20] R. J. Kind and M. G. Potapczuk, "Experimental and computational simulation of in-flight icing phenomena," *Progress in Aerospace Science*, vol. 34, no. 5-6, pp. 257–345, 1998.

[21] Y. Li, C. Sun, Y. Jiang, and F. Feng, "Scaling method of the rotating blade of a wind turbine for a rime ice wind tunnel test," *Energies*, vol. 12, no. 4, pp. 627–627, 2019.

[22] Y. Li, C. Sun, W. F. Guo, S. L. Wang, F. Feng, and Y. Jiang, "Design of icing wind tunnel experiment system for rotating blades by using natural low temperature," *Journal of Experiments in Fluid Mechanics*, vol. 32, no. 2, pp. 40–47, 2018, (in Chinese).

[23] C. Sun, Y. Jiang, and Z. Xu, "Installation angle on icing distribution of rotating blade by Icing wind tunnel Test," *Journal of Engineering Thermophysics*, vol. 40, no. 12, pp. 2815–2821, 2019, (in Chinese).